

Iterative modelling of AEM data based on a priori information from seismic and borehole data

Anne-Sophie Høyer^{1,2}, Flemming Jørgensen¹, Holger Lykke-Andersen² and Anders Vest Christiansen^{1,2}

¹ Geological survey of Denmark and Greenland (GEUS), Ø. Voldgade 10, DK-1350 Copenhagen K., Denmark

² Department of Geoscience, Aarhus University, Høegh-Guldbergs Gade 2, DK-8000 Aarhus C, Denmark

Received April 2012, revision accepted January 2014

ABSTRACT

Airborne electromagnetic methods (AEM) have become an important part of groundwater mapping in a wide range of geological settings. However, as for all geophysical methods, the results of the inversions are non-unique and it is therefore relevant to include a priori information in order to obtain the most realistic geological inversion outcome. Despite the extensive use of AEM, only a few studies describe the effect of including a priori information in large-scale AEM surveys. In this study, ancillary information from seismic and borehole data are used as a priori information. The basis for the study is a densely spaced airborne transient electromagnetic dataset (SkyTEM) from a 100 km² area in the western part of Denmark. Six different inversions are performed, and these are formulated as blocky and smooth inversions with different amounts of a priori information in the deepest part of the sections. The use of a priori information has a significant influence on the interpretation of the sections in the lowermost part of the sequence. Furthermore, the middle part of the sections, which are not constrained by the a priori information, show a significant change through the different inversions. Thus, the study shows that the inclusion of a priori information to the deeper part, significantly enhances the understanding of the geology both in the intermediate and deep levels.

INTRODUCTION

Since the 1990s dense geophysical data sets have become more important in the mapping of groundwater resources and, in this respect, airborne electromagnetic surveys have been increasingly used in a wide range of geological settings worldwide (Sengpiel and Siemon 1997; Gabriel *et al.* 2003; Steuer *et al.* 2008; Supper *et al.* 2009). In order to optimally organize a geophysical survey, available knowledge of the specific geological setting is typically utilised (Pullan 2004) and often, a combined use of different geophysical methods are applied (Jørgensen *et al.* 2003a). In this way, the geophysical methods are selected based on the geological setting in question, and the lateral spacing of measurements are chosen based on the expected geological heterogeneity. However, while the geological knowledge is commonly used to plan the best survey strategy, it is rarely implemented in the geophysical inversions. Therefore, when it comes to data handling, the geophysicist and the geologist typically work independently of one another.

The use of a priori information becomes important as the demand for more user-friendly geophysical results increases. As a consequence of the non-unique nature of geophysical inver-

sions (Tikhonov and Arsenin 1977), the incorporation of ancillary information is relevant in order to obtain the most geologically realistic geophysical model within the range of possible models. The advantages of using a priori information have been discussed thoroughly for many years (e.g., Tikhonov and Arsenin 1977; Jackson and Matsu'ura 1985; Ellis and Oldenburg 1994; Meju 1994; Scales and Tenorio 2001). While some studies describe the implementation of a priori information derived from seismics in traditional transient electromagnetic (TEM) surveys (Shtivelman and Goldman 2000; Nyboe *et al.* 2010), only a few studies with Airborne EM (AEM) data have been conducted (e.g., Teatini *et al.* 2011; Burschil *et al.* 2012; Sapia *et al.* 2012). Of these, Burschil *et al.* (2012) and Sapia *et al.* (2012) implemented information from high-resolution seismics, whereas the seismic data in the study of Teatini, *et al.* (2011) were of very high resolution and therefore only provided information down to 10–20 m of depth. The studies generally show good results when incorporating a priori information from seismics in the AEM inversions. Furthermore, a number of studies describe the use of other sources of a priori information in AEM data, including Brodie and Sambridge (2006), who described a holistic approach for simultaneously calibrating, processing and inverting frequency-domain electromagnetic data together with relevant a priori

information in the form of conductivity and interface-depth data. According to Brodie and Sambridge (2006), this approach ensured a fast procedure with results that were superior to the output of conventional 1D inversion of final processed data.

This paper is a continuation of a study conducted in a study area in the western part of Denmark, where a dense geophysical data set has been collected (Høyer *et al.* 2011; Høyer *et al.* 2013a). In Høyer *et al.* (2013a), the results of the geophysical data set that consists of AEM, high-resolution seismics, geoelectrical and ground penetrating radar data are used to discuss the challenges in mapping the glaciotectionic structures present in the study area. In Høyer *et al.* (2011), the airborne electromagnetic and high-resolution seismic data were compared, and the interpretational benefits from combining these data types were discussed. It was found that the airborne data provided valuable 3D-information on the subsurface, whereas the seismic data delivered more detailed structural information along 2D profiles. The comparison of data furthermore revealed that the initially conducted AEM inversion did not resolve the lowermost part of the layer sequence sufficiently. The results of this study therefore formed the background for studying the effects of including a priori information in order to obtain more geologically realistic SkyTEM inversions. Thus, in this paper, an

iterative approach is used to formulate the most appropriate settings for the inversions based on the ancillary information from seismic and borehole data. In this context, soft a priori information is defined as an unconstrained change of the starting models, whereas hard a priori information is defined as actual constraints, in which the model parameters are constrained to a given value within a defined variance. Both types of a priori information are used in this study, in which the a priori information is based on data from an investigation borehole and high-resolution seismic lines in the study area.

GEOLOGICAL CONTEXT

The study area covers approximately 100 km² and is located in the western part of Jutland, Denmark (Fig. 1). The deposits that are within the focus depth of the SkyTEM data are of Paleogene to Quaternary age. Within the study area the Paleogene sediments consist of marine heavy clays and marls (Larsen and Sand-Jensen 2006). The deposits from the Miocene directly underlie the Quaternary sediments and consist of clay, silt and sand material of marine, deltaic and fluvial origin (Rasmussen *et al.* 2010). The Quaternary deposits consist of glacial tills and interglacial lacustrine sediments. The present-day surface reflects the old Saalian

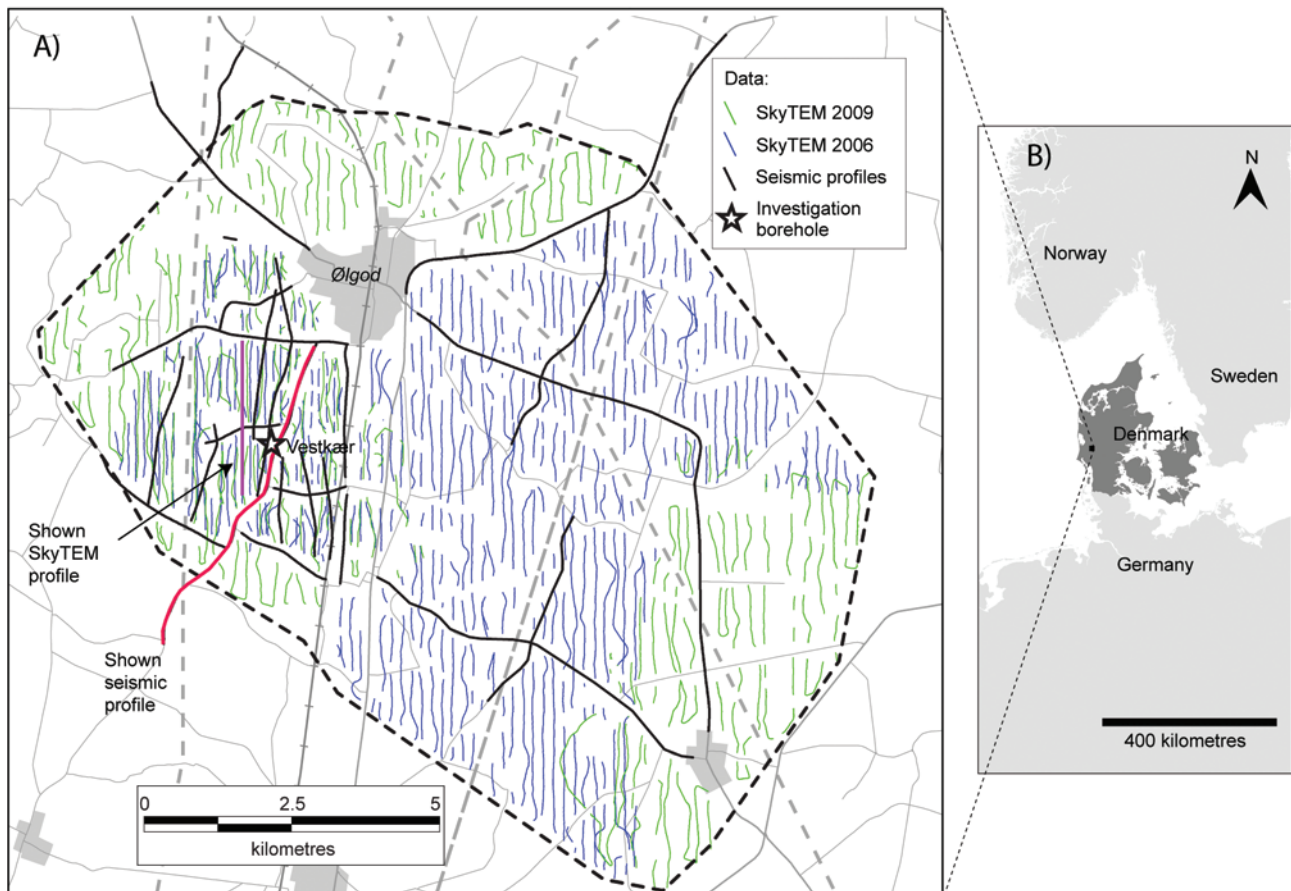


FIGURE 1
A: Data in the study area; B: Position of the study area in the western part of Denmark.

landscape, which has been subjected to various erosional processes during the later Quaternary (Houmark-Nielsen 2004). For instance, deposits from former clay pits in the area (Andersen 1965; Rasmussen 1966; Larsen and Kronborg 1994) and the geophysical data (Høyer *et al.* 2013a) generally indicate an influence by glacio-tectonic processes. According to the boreholes in the area, the sediments are saturated by freshwater, and expected formation resistivities are therefore consistent with typical values obtained in Danish sedimentary environments (Jørgensen *et al.* 2003b).

SKYTEM METHOD

The SkyTEM method is an airborne transient electromagnetic method, where the data are collected from a helicopter on which the entire system is carried as an external sling load (Sørensen and Auken 2004). The data comprise both raw data soundings together with navigation data that are used in the processing and inversion procedure. The voltage data is recorded as db/dt data, but are typically shown as ‘apparent resistivity curves’. The TEM soundings alternate between a low and a high transmitter moment in order to obtain sufficient resolution of both the near-surface layers as well as the deeper layers. The processing of the SkyTEM data is typically conducted according to the recommended approach by Auken *et al.* (2009a), which includes a thorough manual assessment for artificial couplings in the voltage data. The data handling is conducted using the Aarhus Workbench (Auken *et al.* 2009b). The inversion methodology is a full non-linear least squares inversion (see Appendix 1).

Information on the lateral and vertical coherency in the underlying geological structures are added through vertical and lateral constraints as described in (Auken *et al.* 2005) and (Viezzoli *et al.* 2008) and used in various surveys like (d’Ozouville *et al.* 2008; Viezzoli *et al.* 2009; Kirkegaard *et al.* 2011). A priori information can be added to any model parameter including a user-defined uncertainty. The numerical quality of the inversion result is evaluated against the data residual, or data misfit, which is normalized with the noise on the data, meaning that a data misfit of less than one indicates that data are fitted within the ascribed noise and vice versa for a misfit larger than one. When initiating the inversions the actual influence of the starting conditions is dependent on the number and uncertainty of data-points at the soundings in question. Thus, the starting models and their constraints will have a stronger influence on model parameters that are poorly resolved, i.e. where the data carry little information on the given parameter.

Model equivalences are important to consider, due to data uncertainties allowing a number of models to fit the data within the noise level. Though, for EM methods the equivalences are generally less pronounced compared to e.g., DC methods, because of the high sensitivity towards conductive layers and the depth to these layers (Christiansen *et al.* 2006). On the other hand, a model parameter can be resolved, but at the same time poorly determined as is often the case with high-resistivity layers. Equivalence problems are minimized when adding ancillary

information to the data either through lateral and vertical constraints or directly by a priori information from boreholes or seismic data.

In connection with the SkyTEM inversions, the depth of investigation (DOI) is typically calculated using the method of Christiansen and Auken (2012), and we used an absolute threshold value of 0.8 as suggested in the original paper. This methodology is based on the sensitivity matrix of the final model and takes into account the actually measured data and their uncertainties. Assuming that the model fits the data, the method gives the depth above which the individual models are considered data-driven. This allows the interpreter to distinguish between model structures determined solely from the data from structures that depend on other inputs such as a priori information and lateral and vertical constraints. The DOI itself is of course highly model dependent and will vary over a survey, so that it will be deep when a resistive structure overlies a conductive and shallower with the opposite situation.

To gain deeper insight into the resolution and determination of model parameters, a model sensitivity analysis can be computed that allows the interpreter to assess the determination of individual model parameters (Tarantola and Valette 1982; Auken *et al.* 2005). This will allow detailed assessment of, for example, model equivalences, which is not covered by the DOI. For blocky (few-layer) inversions, which are overdetermined (more data than model parameters) the analyses can be used quantitatively, whereas it is only of qualitative use in underdetermined models, like the smooth (multi-layer) models (Menke 1989). Though, for large-scale airborne surveys it is not common to show these analyses for the entire area. In this study we will show examples of the analyses on selected blocky models.

VIBROSEISMIC METHOD

In the vibroseismic method, pulses of controlled seismic energy are emitted from a vibratory source, and the energy in the form of seismic waves, move spherically away from the source. In the subsurface the waves are reflected, when they reach boundaries with marked contrasts in acoustic impedances (defined as the product of density and seismic velocity of the material). The boundaries can constitute lithological changes, but can also indicate other changes like unconformities, changes in water content, etc. (Høyer *et al.* 2011).

In order to enhance the efficiency of data collection of vibroseismic data, land-streamers that consist of cables with attached geophones have been developed (van der Veen *et al.* 2001; Vangkilde-Pedersen *et al.* 2003). The processing sequence aims at improving the signal-to-noise ratio in the final reflection seismic profile, and entails a range of steps, which vary according to the environment. Typically however, the processing includes the following steps; import of field geometry, trace editing and muting, velocity analyses, application of residual statics, normal moveout correction, CMP stacking, migration, bandpass filtering and automatic gain control (Yilmaz 1987).

DATA

SkyTEM data

The SkyTEM data were collected during two mapping campaigns: In 2006, where 174 line kilometres were collected in the westernmost and easternmost part of the area, and in 2009, where 418 line kilometres were collected in the central part (Fig. 1A). The internal line distance varies from 125 m in parts of the 2009 data set to 270 m in the 2006 data set.

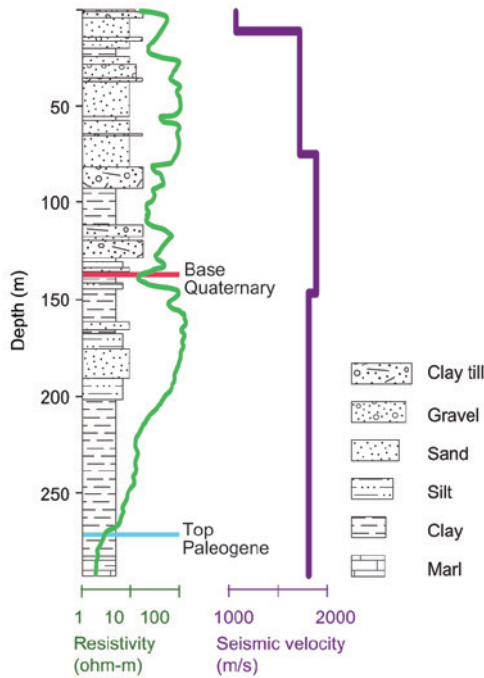


FIGURE 2
The lithological log shown together with the resistivity log (note: logarithmic scale) and the seismic velocities from the vertical seismic profile. Positions of the Base Quaternary and the Top Paleogene horizons are marked on the lithological log.

Analysis of data from the first mapping campaign revealed that the descending tendencies of the sounding curves only were recognized on the very last time-gates (Høyer et al. 2011). The number of usable time-gates proved to be vital for the resolution at depth, and the 2009 survey was therefore collected using a larger high-moment (188000 Am²) than the one used in the 2006 survey (113000 Am²). As a result, the last usable gates in the 2009 survey, correspond to 5–6 ms after the beginning of turn-off compared to 2–3 ms after the beginning of turn-off for the 2006 survey.

Seismic data

During 2008 and 2009, a total of 77 kilometres of vibroseismic lines were recorded within the study area (Fig. 1A). Most of the lines (60 km) were recorded along roads, using a land-streamer setup (Vangkilde-Pedersen et al. 2003; Vangkilde-Pedersen et al. 2006), whereas the remaining lines were recorded on cultivated fields with a traditional split-spread configuration.

The seismic data were processed in a traditional scheme leading to CMP (common midpoint) stacked sections (Yilmaz 1987). The stacked sections were depth converted based on two intervals of mean seismic velocities, obtained from the results of the vertical seismic profile (Fig. 2).

The seismic interpretations were conducted in a traditional manner in which characteristic reflections were interpreted based on visual inspection of the profiles (Fig. 3). The lithological and palynological information (Dybkjær 2011) from the investigation borehole (Fig. 2) was used to relate the interpreted horizons to stratigraphic changes.

Borehole data

Data from approximately 600 boreholes are available within the study area. However, the boreholes are generally very shallow and only 10 % are deeper than 60 m. Furthermore, the quality of the borehole descriptions is highly variable. Therefore, in order to obtain reliable borehole data at depth, a new investigation

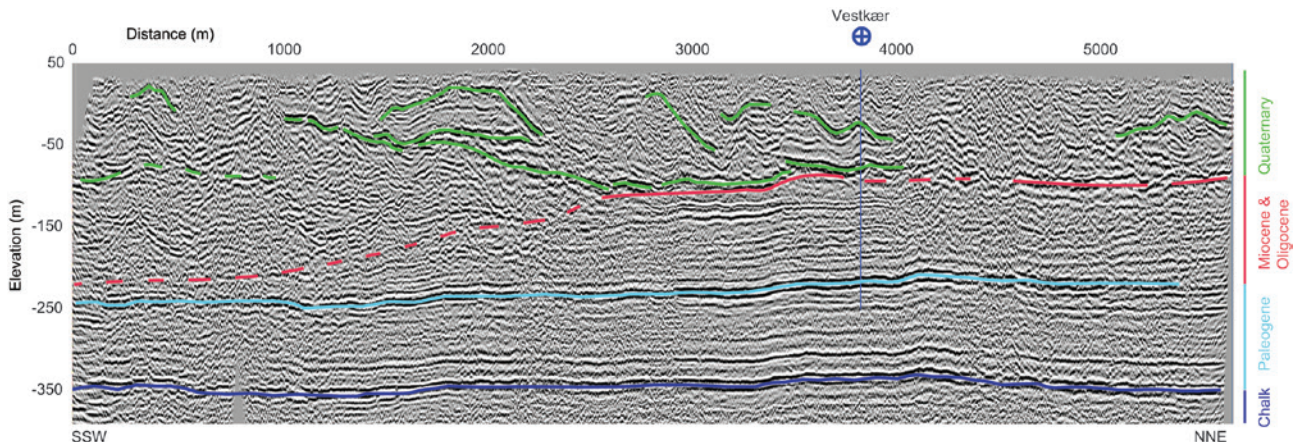


FIGURE 3
The seismic line close to the investigation borehole ('Vestkær'), see Fig. 1 for location. Vertical exaggeration = 4x. The lowermost three reflections mark the interpreted reflections 'Top Chalk' (dark blue), 'Top Paleogene' (turquoise) and 'Base Quaternary' (red). Internal reflections in the Quaternary section are marked with green.

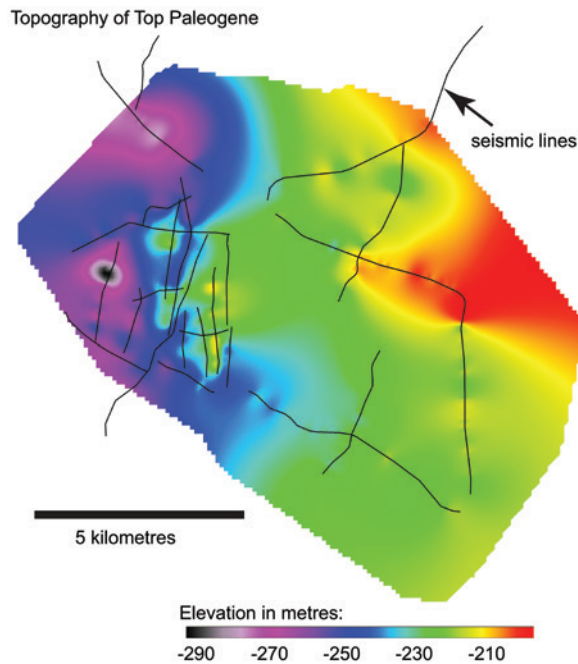


FIGURE 4
Grid showing the elevation of the Top Paleogene surface in the SkyTEM covered area. The grid is based on the seismic interpretations. The seismic profiles are shown as black lines.

borehole ('Vestkær') was drilled in 2009. The borehole was placed close to one of the seismic lines (Fig. 1) and was drilled to a depth of 294 m (Fig. 2). The reverse, air-lift circulation drilling technique was used and lithological samples were collected and described for every metre. Furthermore, 12 samples from the lower part of the borehole were subjected to palynological analyses for more precise dating (Dybkjær 2011). A number of different logs including resistivity and vertical seismic profiling were also conducted in the borehole (Fig. 2).

GEOLOGICAL OBSERVATIONS MADE ON SEISMIC AND BOREHOLE DATA

All available data from the area show a high degree of heterogeneity in the Quaternary sequence. Information from the investigation borehole was used to assist in the delimitation of the Pre-Quaternary from the Quaternary. On the seismic data, the change from the deeper, largely horizontal and continuous reflection pattern to a more chaotic pattern at shallower depths is interpreted as the boundary between the Quaternary and Miocene strata (Fig. 3). The distinct thrust structures observed in the Quaternary strata are the likely result of glaciotectonic processes (Høyer *et al.* 2013b). According to the seismic observations, the thickness of the Quaternary sequence is 100 to 200 m (Fig. 3).

In accordance with the seismic data, boreholes in the study area show a high degree of complexity and lateral lithological variation in the Quaternary section. Many boreholes also show interbedded sequences of Miocene and Quaternary deposits.

However, this is not observed in the investigation borehole, "Vestkær". The Quaternary sequence in the Vestkær borehole, consists of sedimentary layers with different grain sizes (Fig. 2). The Base Quaternary was identified from palynological analyses (Dybkjær 2011), as this was not obvious in the lithological samples. Most of the pre-Quaternary sediments are composed of marine Miocene deposits. The lower Miocene section (200–272 m) consists of clayey sediments that show a decrease in resistivity from around 50 Ω m to 5 Ω m with depth. The decrease is most pronounced in the upper part of the Miocene section, and from around 230 m of depth, the resistivity log shows more constant values from around 10 Ω m to 5 Ω m. The lowermost part (272–294 m) of the borehole is comprised of Paleogene clays and marls that, according to the resistivity log, show very low values, in the order of 2–3 Ω m. This is consistent with direct resistivity measurements of the Paleogene deposits in the borehole that show a mean value of 2.5 Ω m.

On the seismic data, the pre-Quaternary sequence appears homogeneous, with continuous reflections that show a smooth westerly dip. Two distinct pre-Quaternary horizons, the 'Top Chalk' and the 'Top Paleogene', were interpreted throughout the study area, and the position of the Top Paleogene reflection was verified in accordance with the observations in the investigation borehole (Fig. 2). Both horizons are recognized as easy-interpretatable seismic reflections that show only little topography. As a consequence of the smooth topography, it is acceptable to use the seismic information to construct a grid of the Top Paleogene surface (Fig. 4), despite the difference in seismic data density. The grid shows that the Top Paleogene dips from elevations around 210 metres below sea level (mbsl) in the eastern part to elevations of 270 mbsl in the westernmost part of the area. Since the terrain is around 50 m above sea level, the Paleogene clays are therefore present down to depths of 320 m, which is exceeding the penetration depth of the SkyTEM method in this survey. Due to the varying spacing of the seismic lines, the grid shows a higher degree of detail in the western area, where the data density is highest.

SKYTEM INVERSIONS

The total data misfits of the inversions are listed in Figure 5, which also presents a plot of the data misfit of the first (a smooth 25-layer model) and the last SkyTEM inversions (smooth 30-layer inversion with a priori information) conducted in this study. The inversion results are presented on a north-south striking profile in Fig. 6A-F. The data and modelling results for one of the SkyTEM soundings in the profile are shown in Fig. 7A-F. Finally, the inversion results are also shown in 3D fence diagrams in Fig. 8A-F. In Fig. 6 the SkyTEM models are presented as stitched 1D soundings along a profile that follows a SkyTEM flight-line (buffer 25 m), and the misfit and DOI's of the models are therefore also plotted in this figure. The profile represents a typical example from the western part of the study area, and is also utilized to illustrate the changes imposed on the geological interpretations, when adding knowledge from the different inver-

sions in Figure 9A-F. In Figure 8, the fence diagram shows four north-south striking profiles and three east-west striking profiles, seen from the south-west. These profiles show interpolated resistivity data based on the SkyTEM soundings. This figure is used to illustrate the regional outcomes of the iterative inversion steps.

Smooth 25-layer model

The first inversion that was conducted in the study area was a smooth inversion with 19 layers, which was performed with settings that corresponded to standard settings for a typical Danish geological environment (Høyer *et al.* 2011). In order to avoid a change of the degree of detail in the near-surface (thickness of layers) when comparing this model with a smooth model with deeper discretization, we conducted a corresponding 25-layer model, which is the one presented here. The depth to the last layer boundary was estimated to 250 m based on the typical maximum depths of penetration of the SkyTEM method. The vertical distribution of layers was chosen, such that the thicknesses increased logarithmically from 5 m in the first layer to 17 m in the last layer. Being a smooth inversion, the thickness of layers remained fixed and vertical constraints controlled the degree of resistivity variance between layers internally in the models, whereas horizontal constraints of the SCI controlled the variations between neighbouring models. The resistivities were started at 40 Ωm and the vertical constraint on the resistivity was defined as 2.5. The horizontal

constraints were tightened from 1.6 in the upper part to 1.2 in the deepest part as a consequence of the decrease in resolution of the SkyTEM method with depth. The constraints do not impose fixed limits on parameter changes, but rather act as rubber bands, and a constraint number of 1.2 can be thought of as an allowed variability on the model parameters of 20% between the constrained models. The exact values for constraints are based on experience from a large number of surveys combined with the expected geological heterogeneity. The total noise-normalized data residual for the inversion was 0.741 (Fig. 5), indicating that the data were generally well-fitted within the noise level of the data. Therefore, the model is fully acceptable when considering the data fit and, without other sources of information, this model could easily be accepted. The distribution of the average data residual illustrates the difference between the information in the data sets from 2006 and 2009, respectively. Hence, within the well-fitted range (< 1) data residuals are generally a little higher in areas with 2006 data (0.7–1) compared to areas with 2009 data (< 0.7) (Fig. 5).

The topmost part of the SkyTEM sections (Fig. 6A,) shows a high degree of complexity, in which resistivity changes occur gradually. The sections have a smooth appearance and the shape of the structures resemble the forms that are recognized in the seismic data (Høyer *et al.* 2011). However, in the lower part of the sections, there are significant discrepancies between the inversion results and the information from the seismic data and

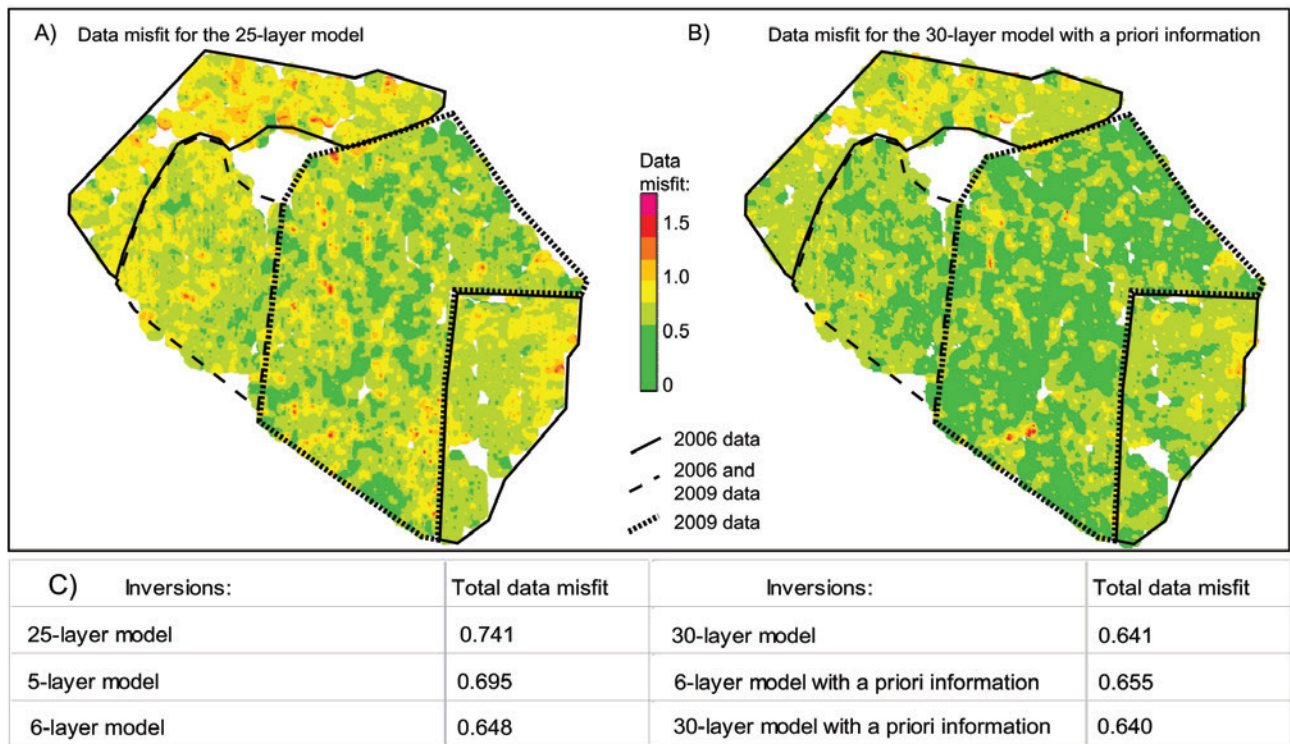


FIGURE 5

Data misfits for the different inversions. In A and B the areas for the different survey campaigns are marked. A: Gridded data misfits for models from the 25-layer inversion. B: Gridded data misfits for models from the 30-layer inversion with a priori information. C: Total data misfits shown for each inversion.

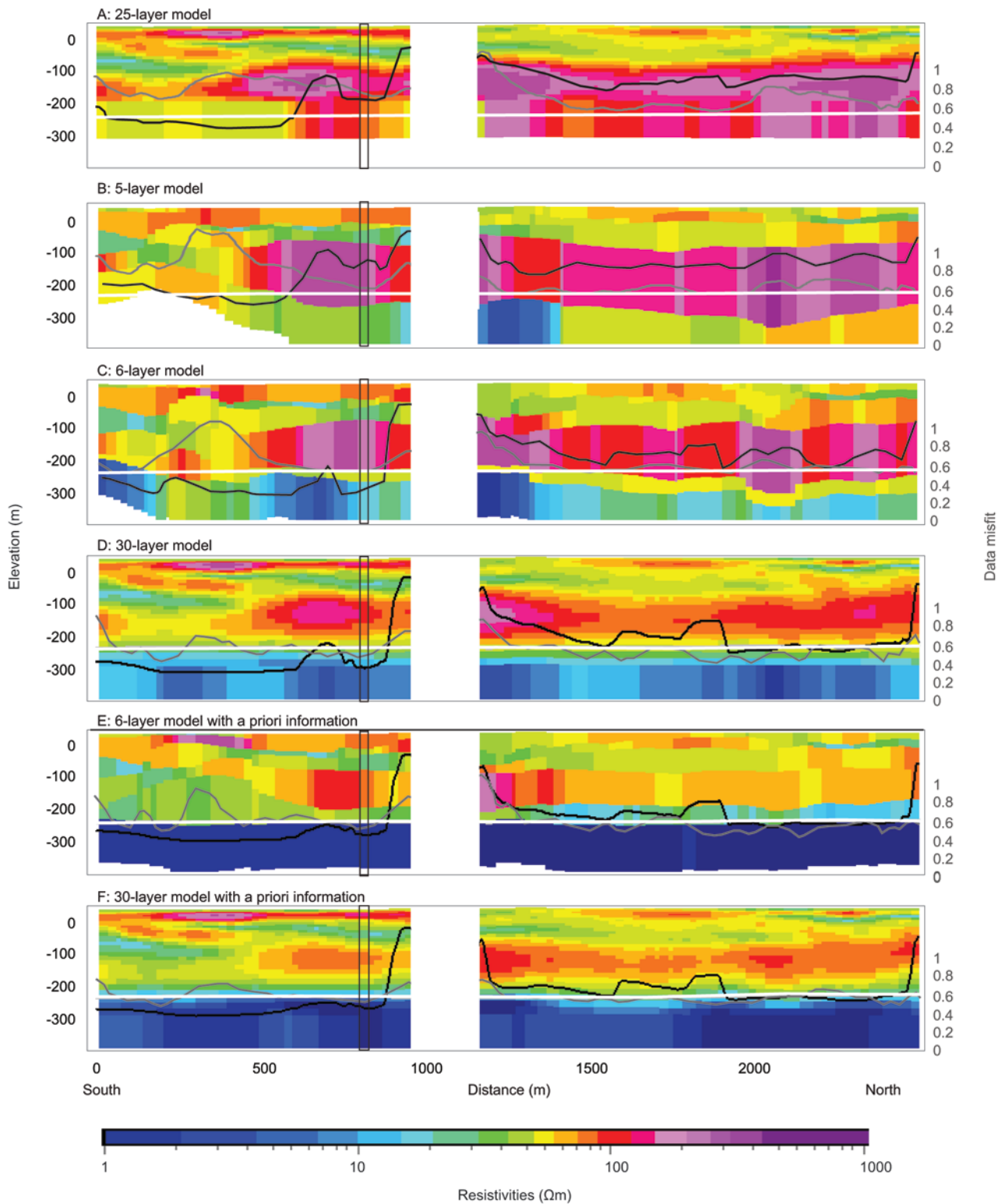


FIGURE 6

Results of the different inversions. Stitched 1D models along a S-N striking flight-line in the western part of the area (buffer 25m). The data misfits are shown with grey, the DOI's (Depth of Investigation) are shown as black lines and the Top Paleogene grid (Fig. 4) is shown as a white line. The black boxes on the sections mark the position of the model for which data are shown in Fig. 7. The position of the profile is shown in Fig. 1A.

the borehole (Høyer *et al.* 2011). Here, the SkyTEM data shows resistivities that vary considerably at great depth in the western part of the area (Fig. 8A), which is inconsistent with the expected presence of a continuous good conductor. At the same time, the DOI calculation shows that there are significant differences in the depth of investigation within the area. Thus, the DOI is typically placed at relatively deep levels (~ 200–300 mbsl) in the eastern part of the area compared to significantly shallower depths (~ 50–200 mbsl) in the western and northern parts.

5-layer model

Based on the information obtained from the seismic data and the boreholes, a good conductor is expected to be present in the entire study area. In order to evaluate whether a good conductor was detectable at greater depths than the depths discretized in the 25-layer inversion, a blocky inversion was conducted. The shown inversion was performed using five layers, since it was established that at least five were necessary to mimic the heterogeneous geological setting. Thus, the starting model was discretized

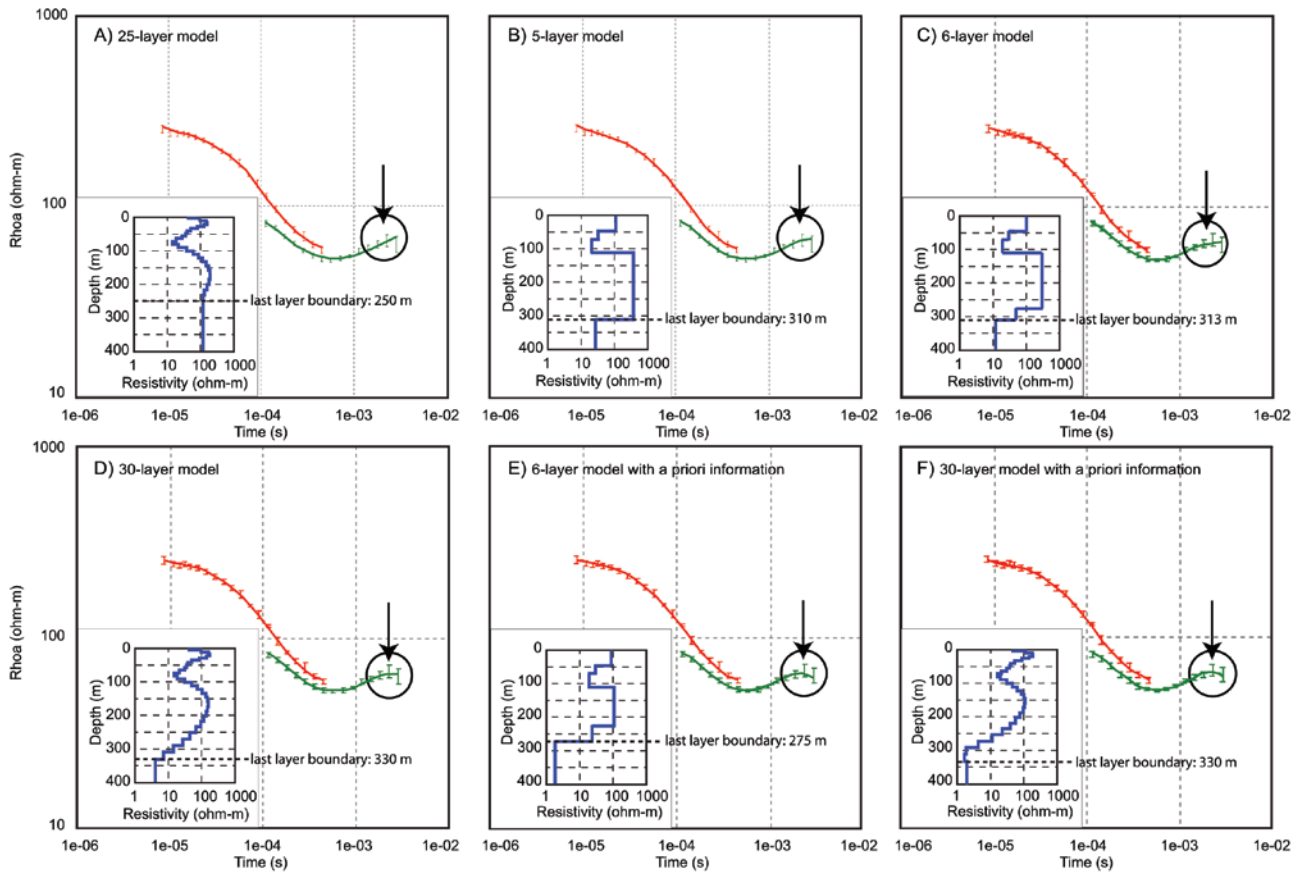


FIGURE 7

Example on a sounding (marked in Figs 6A-F), fitted with the six different inversion results (A-F). The data are shown with uncertainty bars (red are low-moment data and green are high-moment data), and the curves illustrate the inversion results. The four last data points are marked in order to highlight the differences between the model results. Inserts in the lower left show the model results. The model parameter analyses of the blocky models (B, C and E) can be seen in Table 1.

TABLE 1

The model parameter analyses of the blocky models shown in Fig. 7(B, C and E). For each model, the upper row shows the modelled values (height of the transmitter frame, thickness, resistivities and depths), while the grey shaded rows show the standard deviation factors (STDF). STDF values above 3 are marked with asterisks (*). Improvements in the estimation of model parameters are marked with green.

	TxZ	Res_01	Res_02	Res_03	Res_04	Res_05	Res_06	Thic_01	Thic_02	Thic_03	Thic_04	Thic_05	Dep_01	Dep_02	Dep_03	Dep_04	Dep_05
5 layer (B)	30,5	100,2	31,5	19,2	328,6	25,1		46,8	22,3	40,1	200,4		46,8	69,1	109,2	309,6	
	1,01	1,03	2,49	2,23	*	*		1,24	*	*	2,52		1,24	1,74	1,50	1,36	
6 layer (C)	30,5	102,6	29,9	19,4	288,3	49,7	12,1	47,3	23,7	40,1	167,1	34,9	47,3	71	111,1	278,2	
	1,01	1,03	2,42	*	*	*	*	1,22	*	*	*	*	1,22	2,20	2,82	*	*
6 layer	30,5	103,4	31,7	19,6	112,9	27,4	2,2	45,9	20,8	45,2	118,4	44,4	45,9	66,7	111,9	230,3	
apriori (E)	1,01	1,04	2,66	2,08	*	*	*	1,27	*	*	*	*	1,27	1,70	1,71	*	2,50

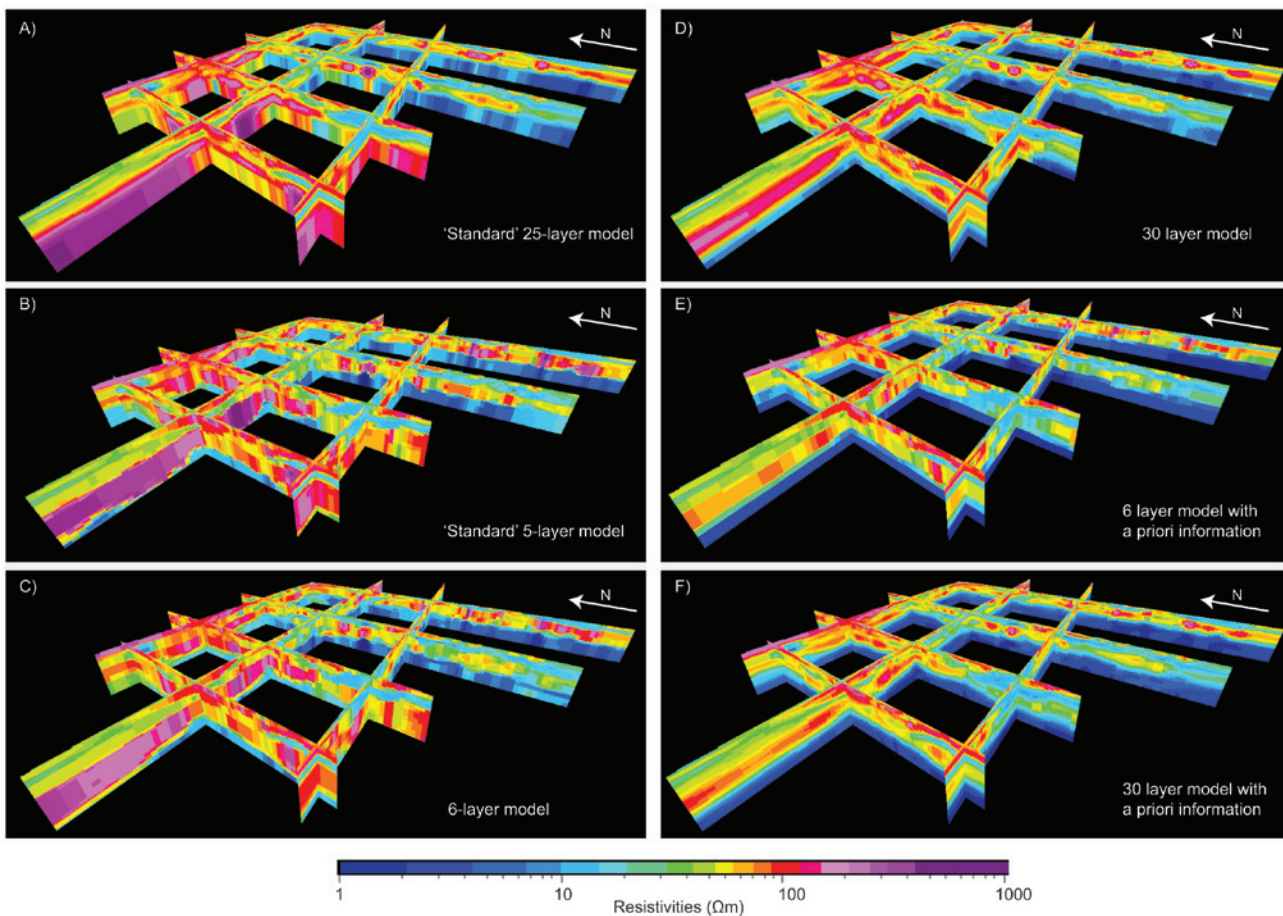


FIGURE 8

3D fence diagrams showing the SkyTEM results of the six different inversions. Each fence shows three E-W striking profiles and four N-S striking profiles. The fences are seen from a south-western direction.

with layers of increasing thicknesses (from 25 to 75 m), and with 40 Ωm as the starting resistivity value for all layers. The values were rather free to change during the inversion, since only starting values and no vertical constraints were defined for the depths and resistivities. However, in order to control the fluctuation of layer boundaries and resistivity values between neighbouring models, lateral constraints favouring horizontal layers were used. Thus, the constraints on the resistivities normalized with the distance corresponded to 1.5 (layer 1–4) and 1.4 (layer 5), whereas the normalized lateral depth constraints were tightened with depth from 1.5 in the first layer to 1.044 in the fourth. Again, the tightening of the constraints with depth was conducted as a consequence of the decrease in resolution of the SkyTEM method with depth.

The upper part of the model results show a heterogeneous resistivity pattern (Figs 6B, 8B), which appears rather crude and, in general, it is difficult to recognize the structures that are known from the seismic data. At depth, the inversion consistently shows a good conductor in the eastern part of the area (Fig. 8B). Likewise, the majority of the models from the western

part indicate the presence of a relatively good conductor which, however, is located at great depths and in many places exceeds the depth to the Paleogene, as interpreted on the seismic data (Fig. 4). In summary, the resistivity level and depth to the boundary of the Paleogene are relatively constant in the eastern part of the area, whereas both parameters are highly variable in the western part (Figs 6B, 8B).

In this respect, the blocky model shows that there is some, albeit limited, sensitivity in the data towards a good conductor in the entire area. Furthermore, the model shows that the good conductor appears to be present at greater depths than the last layer boundary in the 25-layer inversion. However, the model indicates more variable depths and resistivities than expected from the seismic data.

6-layer model

In order to mimic the heterogeneous geological setting better, it was of interest to use a model with as many layers in the blocky inversion as possible. It was therefore investigated whether the data information was sufficient to resolve the parameters in a six

layer inversion. The layers in the model were started with increasing thicknesses from 20 m in the first layer to 85 m in the fourth layer. However, the fifth layer was started with a relatively small thickness compared to the depth (40 m), as a consequence of the information from the borehole (Fig. 2), which shows a 40 m thick layer above the Paleogene clays that shows a characteristic resistivity value. However, in order to avoid a priori information on the resistivities at this stage, all the layers were started with resistivities of 40 Ωm , and were free to change during inversion. The constraints on the lateral resistivity variations and depths correspond to the constraints in the five layer model.

The upper part of the model results show a heterogeneous resistivity pattern (Fig. 6C), which resembles the structures mimicked in the 5-layer inversion. As for the first two inversions, this inversion also shows a good conductor in the eastern part of the area (Fig. 8C), whereas the resolution of a good conductor is more uncertain in the western part. The most significant difference between the 5-layer and the 6-layer inversion is the occurrence of a relatively thin layer with immediate resistivities below the high-resistive unit (around 280 to 300 mbsl in Fig. 6C). Apparently, the data information is sufficient to resolve the parameters of the 6-layer inversion in most of the area, and the inversion generally shows a total data misfit (0.648, Fig. 5C) that is marginally better than the 5-layer model (0.695, Fig. 5C).

The inversion indicates that it is too simplified to describe the heterogeneous geological setting with a 5-layer inversion. Originally, this was also the background for handling the SkyTEM data with a smooth inversion, but apparently the first smooth model was conducted using too shallow discretisation.

30-layer model

The information from seismic data and the results of the blocky inversion suggest that the smooth model needs a deeper discretization in order to enable a possible resolution of the good conductor at depth. A 30-layer model was therefore established with deeper discretization than the initial smooth model, but with the same starting resistivities and vertical constraints on resistivities. 30 layers were used in order to obtain an equivalent smooth model in the near-surface, while adding layers in the deeper part (down to 330 m of depth). This depth was chosen as it exceeds the expected maximum depth of the Paleogene surface in the entire area (Fig. 4). The total data misfit shows an improvement (0.641) compared to the misfit of the 25-layer model (0.741) (Fig. 5C), which indicates that the deeper discretization of the 30-layer model provides a marginally better model space.

With the exception of a few areas in the western part, the deep-lying good conductor is now resolved in most of the area (Fig. 8D). In addition, the thickness and resistivity of the high-resistive unit above the good conductor is reduced considerably (e.g., Fig. 6D, distance 1500 to 2000 m). However, as a consequence of the gradual resistivity changes of the smooth model, the actual layer-boundary to the good conductor cannot be defined precisely. The upper layer sequence (down to 100 mbsl)

shows smooth resistivity changes, and only a few deviations are observed between the 30-layer and the original 25-layer model in this part of the sequence.

The outcome of the 30-layer model emphasises the fact that the data contains information regarding the presence of a good conductor throughout the majority of the study area. The lack of resolution of the good conductor in the initial 25-layer model therefore stems from a too shallow discretisation of this model. However, the small differences in the data fit (Fig. 5C) and the example showing the sounding curves (Fig. 7A-F), illustrates that the information content of the good conductor is very small in parts of the area. The layer would therefore not have been resolved if the data were inverted as single soundings, as the resolution is dependent on the migration of information through the spatial constraints. The outcome of the inversion emphasises the importance of an adequate discretization of the smooth inversions.

6-layer model with a priori information

In order to obtain a better resolution of the lowermost section, geological observations from the seismic data and the investigation borehole were utilised as a priori information in the 6-layer model. Since the Top Paleogene constitutes a geological boundary, which is recognizable both in the resistivity data by showing resistivity contrast between the materials above and below, and in the seismic data through a marked seismic reflection (Høyer *et al.* 2011), it is possible to use this boundary as a priori information in the inversions. The grid of the Top Paleogene from the seismic data was therefore used as strong a priori information to constrain the elevation of the lowermost good conductor. Despite the significant interpolation distance between some of the seismic lines, the grid is considered usable because the Paleogene surface is known to show little topography in this part of Denmark (Friborg and Thomsen 1999), just as the horizon appears smooth on all the seismic lines in the study area. However, a variance of 10 % from the seismic grid was allowed, because of the relatively large interpolation distance and the uncertainties related to depth conversion of seismic data. On the other hand, the smooth, homogeneous appearance of the Pre-Quaternary sequence formed the basis for further tightening of the horizontal constraints in the lowermost layer of the SkyTEM models (from 1.4 in the first 6-layer inversion to 1.01 in this one). Thus, the layer boundary between the fifth and sixth layer was constrained to the Top Paleogene grid. The sixth layer was started at a resistivity of 2.5 Ωm , but without constraints, so the values were free to vary. At the same time, the borehole information regarding a unit of low resistive Miocene clays on top of the Paleogene were utilised to formulate starting values as soft a priori information for the fifth layer of the model (25 Ωm) (Fig. 2). This value was relatively high, corresponding to the resistivity observed in the borehole for the 40 m interval. However, we used this value to avoid starting the resistivity at such low values that the inversion could not change to higher values if needed.

The inversion results show a good conductor, below the top Paleogene grid with almost constant resistivities (2–5 Ωm), in the

entire study area (Figs 6E, 8E). The layer boundary is generally consistent with the Top Paleogene grid, however, the boundary does not strictly follow the grid in the entire area (e.g., Fig. 6E around 2000 m). The layer just above the grid generally shows relatively low resistivities that are within the range of clayey sediments (e.g., Fig. 6E). Above this interval, the thickness and resistivity of the high-resistive layer appear to be significantly reduced compared to the 5-layer model (e.g., Fig. 6B, 1500–2500 m). In the topmost part, the inversion results show only minor deviations from the other blocky models.

30-layer model with soft a priori information

Finally, in order to incorporate the information from seismics and boreholes into the smooth inversion, soft a priori information was included in the 30-layer inversion. The model was set up similarly to the aforementioned 30-layer model before adding the a priori information. As for the 6-layer model, the a priori information was introduced based on the seismic grid of the Top Paleogene and the resistivities recognized in the resistivity log by the investigation borehole. Hence, starting resistivities of 2.5 Ωm were assigned as soft a priori information to the layers beneath the grid.

The models show a continuous good conductor with resistivities that appear relatively constant in the entire study area (Fig. 8F). Generally, the resistivities of the good conductor are lower than the observed resistivities of the 30-layered model without a priori information. As for the other smooth models, it is difficult to determine precisely the position of the layer boundaries. However, the boundary to the good conductor appears to be slightly closer to the surface compared to the obtained depths in the 30-layer model without a priori information (e.g., Fig. 6D). Thus, the overlying high-resistive deposits experience a further reduction of the thickness compared to the model without a priori information just as the maximum resistivities are further reduced. Note that the reduction of the thickness and resistivities of the high-resistive layer above the good conductor are somewhat counter-intuitive. Thus, one would expect that the increase of conductive material at depth would imply removal of conductive material elsewhere in the model. However, the opposite is seen in this case.

Evaluation of the models

Fundamentally, the issue that initiated this study was the difficulty in resolving the deep-lying good conductor in the western and northern part of the study area as experienced in Høyer *et al.* (2011). This difficulty is a result of the interaction between the geological and the geophysical conditions in the area. As a consequence of the westward dip of the pre-Quaternary sequence, the good conductor is situated at great depths in the western part of the area. At the same time, the instrumental differences between the two mapping campaigns result in significant differences in resolution capabilities. In this geological setting, the number of usable time-gates has a significant influence on the resolution of the good conductor at depth, since the descending

tendency of the sounding curves only is recognized on the very last time-gates (Fig. 2). A few usable data points more or less can therefore be crucial in order to resolve the lowermost part of the sequence, which was demonstrated in Høyer *et al.* (2011) by two synthetic SkyTEM responses produced on the basis of the resistivity readings from the ‘Vestkær’ borehole. Inverting the entire survey as one system by adding spatial constraints enhances the resolution of these layers, by informing the inversion on the lateral homogeneity and thereby combining all the small information packets in the individual soundings.

In the current study, the results of the different inversions represent equivalent models, and from a geophysical perspective, the models are therefore of almost equal validity, which is illustrated by the data misfits that are within the same range for all the inversions (Fig. 5C). The equivalency is also demonstrated by the model fitting of the sounding curves in Fig. 7A–F, where all the model curves fit the data within the noise of the data, but some of the model curves show a slightly better data fit at very late times (e.g., E and F compared to A and B). Also the example with model parameter analyses of the results of the blocky inversions (Table 1) shows how the data are only marginally better fitted, when incorporating the a priori information. The improvements are recognized for the resistivity and depth parameters at large depths (Table 1, marked with green). Model parameter analyses for underdetermined models such as the smooth models are only of qualitative use and are therefore not shown here.

As a consequence of the use of soft a priori information, the actual influence of the a priori information on the outcome is dependent on the number and uncertainty of data-points at the soundings in question. Hence, the models that are based on high-quality data are entirely data-determined and will therefore not change according to the change in starting models. The change of the starting models will therefore only influence the models, which are based on data of poorer quality. In the current study, this is recognized when observing the outcomes of the lowermost section. Thus, almost no changes are observed in the eastern part of the area, whereas significant changes are recognized in the models from the western and northern parts of the area, where the data information at great depths is weaker (Fig. 8).

GEOLOGICAL INTERPRETATION

The inclusion of additional data to the SkyTEM inversions adds to the understanding of the geological environment. The amelioration of the geological model is illustrated in Fig. 9. The figure shows how the geological interpretation of the profile from Fig. 6 changes as the knowledge from the different SkyTEM inversions are added, given that the interpretations are made solely on the inversion results. In this way, the first interpretation (A) is based solely on the smooth 25-layer inversion: From this inversion, inclined structures of sands and clays can be interpreted in the near-surface. These overlie a thick coarse-grained unit that extends to the bottom of the section in the majority of the profile.

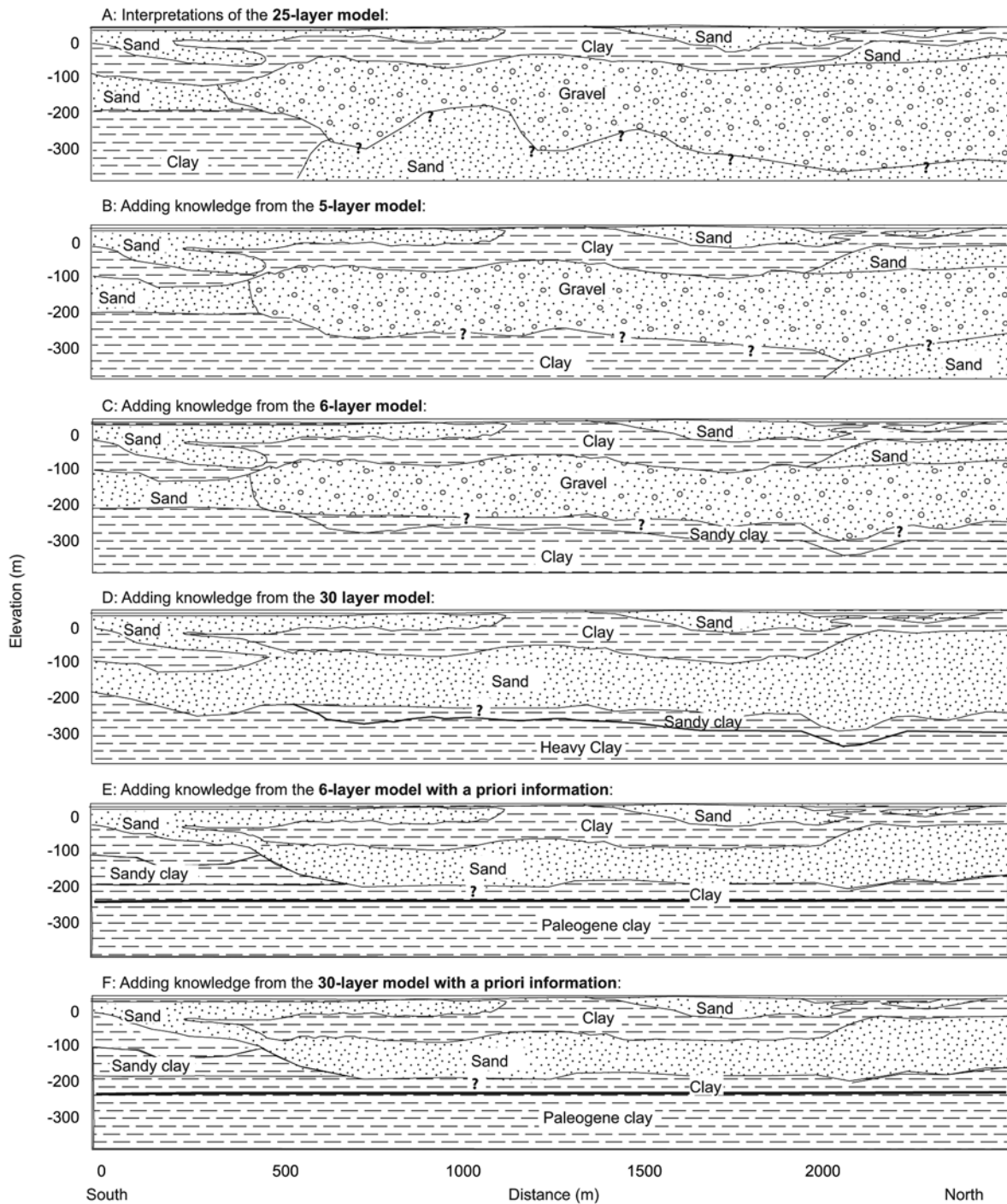


FIGURE 9 Geological interpretations of the SkyTEM profile shown in Fig. 6A-F. The interpretations are made from ‘top to bottom’ such that the cumulative geological knowledge obtained from the different inversions is shown. Thus, the final geological interpretation is shown at the bottom.

In the middle part, the coarse-grained interval shows very high resistivities, which indicate gravelly sediments. However, in the deepest part of the section, the resistivities are slightly lower, and sandy materials are therefore interpreted in this part of the section. At the same time, the even lower resistivities in the south-

ernmost part of the profile formed the basis for interpreting clayey sediments in this area. However, the shallow position of the DOI reveals that the basis for the interpretation of the deeper part of the section is uncertain, which is why question marks are shown in the figure.

The 5-layer inversion contributed to further understanding regarding the lower part of the section. Typically, blocky inversions are good at estimating the precise layer boundaries of good conductors, and in this case, the 5-layer inversion estimates a depth to a good conductor in the majority of the profile. This information is therefore included in the geological interpretation (B). However, according to the DOI, the information at these depths is also uncertain. The structures in the topmost part of the section are not as well-resolved as in the smooth inversion outcome, since the few layers are insufficient to represent the heterogeneous environment. The interpretation of this part is therefore retained from the smooth inversion.

The 6-layer inversion provides information about a thin layer present below the gravelly unit (C). The layer shows intermediate to low resistivities that were interpreted to represent a relatively fine-grained material such as sandy clay. At the same time, the inversion results show more consistently low resistivities of the deepest layer, which has been interpreted to consist of clay in the entire extent of the profile. The changes to the interpretation have been made to the part of the profile that is below the DOI, and are therefore rather uncertain.

The 30-layer inversion provides the smooth transitions known from the smooth model, at the same time as representing the good conductor at great depths (D). The smooth inversions show comparable representations of the topmost sequences and the interpretations of the near-surface are therefore almost unchanged, when considering the different inversions (A-F). However, the interpretation of the intermediate high-resistive unit, and the layers below, experiences significant changes when considering the different inversions. According to the 30-layer inversion, the deepest part of the section consists of heavy clay, whereas the thin layer recognized in the 6-layer model show relatively low resistivities consistent with clay. However, since the layer is present in the transition zone where the resistivities change gradually in the smooth model from the high resistivities above to low resistivities below, the actual resistivity value is best determined by the 6-layer inversion. At the same time, the blocky inversions typically are better at estimating precise depths to layer boundaries, and thus, the position and material (sandy clay) of the layer are not changed from C. The coarse-grained unit above, appears considerably thinner, and the sediments are interpreted to be sandy instead of gravelly.

By introducing a priori information in the blocky inversion, the lower unit can be divided into two independent clay units, in which the lowermost is Paleogene (E). The clay unit on top of the Paleogene is most obvious in the 6-layer model, which provides distinct layer boundaries, compared to the gradual transitions offered by the smooth model. The 30-layer inversion with soft a priori information do not result in any modifications to the cumulative interpretation (F), but if the geological interpretation should be based on a single inversion, this inversion provides the most complete representation. Though, as mentioned above, this

inversion would not be sufficient in order to interpret the clayey unit that overlies the Paleogene clay.

It appears that the altered starting conditions result in outcomes that provide considerable changes to the sections at medium- to great depths. In this way, the coarse-grained interval above the clays appears significantly thinner in the inversions with improved starting conditions, especially when grid and resistivity information are added to the starting models (E-F). In this way, the sandy interval in the final interpretation, shows only half the thickness compared to the initial interpretation.

The differences between the inversions can seem dramatic, however it is important to bear in mind that the model-structures influenced by the a priori information have a very weak imprint on the observed data. This is demonstrated by the subtle difference between the forward responses of the models in Fig. 7. In other words, the range of models is more or less equivalent when judged solely by the data residuals (Fig. 5C). Thus, by adding only a small amount of a priori information, the inversion is guided towards the most likely of the equivalent solutions, from a geological point of view. In this study, the effect of adding a priori information is significant; however, this is not necessarily the case for all geological settings. Nevertheless, the adding of ancillary information will typically direct the inversion towards the most geologically realistic model. However, when applying the a priori information, it is important to evaluate and include the uncertainties of the added information.

DISCUSSION AND CONCLUSION

Different amounts of a priori information have been incorporated in the AEM inversions, and the study illustrates the advantages of considering the present geological environment when setting up geophysical inversions. For instance, significant enhancements of the smooth inversions are observed exclusively as a result of refining the discretisation of the smooth inversions. The a priori information in this study has been implemented both in a blocky inversion and in a smooth inversion. The geological boundary of the Top Paleogene was characterised by physical properties recognizable by both electromagnetic methods in the form of a marked decrease in resistivity and by seismics as a contrast in acoustic impedance (Høyer *et al.* 2011). Hence, this boundary was useful as a priori information to help in delimiting the good conductor. The elevation was derived from the seismics and used to attach low starting resistivity values to the Paleogene deposits. Apart from better simulation of the good conductor, the inversions with soft a priori information showed a change in the above-lying layers, which experienced a significant decrease in both the thicknesses and the resistivity values. This was also recognized by Sapia, *et al.* (2012) where constraints were attached to the lower part in a smooth (19 layer) inversion. Apart from better representing this boundary, the inversion furthermore showed more resistive deposits and lower uncertainties for the resistivity values in the overlying layers.

In this study, we have demonstrated how the end product, in this case the geological interpretation, changes when adding knowledge from different inversions. Apart from the importance of using ancillary information in the SkyTEM inversions, the study also demonstrates the advantages of operating with blocky inversions together with smooth inversions. Complex geological environments are often indescribable by only a few model layers, which is why smooth models can be necessary to provide a realistic visualisation of the geological setting. However, blocky models are still relevant in order to provide information of the more exact position of the main layer boundaries, and the outcomes can advantageously be used to support in choosing adequate discretisation of the smooth inversions.

The inclusion of a priori information resulted in considerable improvement in the geological understanding compared to the initial SkyTEM inversions. The influence of the changed starting conditions in this study seem to be more pronounced than in the studies of Burschil *et al.* (2012) and Sapia *et al.* (2012). This is in agreement with the expected, because of the sparse data information present at the depths, where the a priori information is utilised in this study. Thus, the inversion outcome only differs slightly in areas with strong information in the data, whereas it varies significantly in areas with vague data information.

ACKNOWLEDGEMENT

The project is funded by the Geological Survey of Denmark and Greenland, (GEUS), the Faculty of Science at University of Aarhus, and the Nature Agency in Ribe. We would like to thank the crew of students, who assisted in the field with seismic data collection, Per Lynnerup Trinhammer for seismic engineering, Egon Nørmark for seismic processing, and Esben Auken, Bjarke Roth and Nikolaj Foged for assistance on SkyTEM data handling. Furthermore, we appreciate the comments from two anonymous reviewers, who helped refining the paper. Finally, we would like to thank Eoin McGregor for improving the English language of the paper.

REFERENCES

- Andersen S.T. 1965. Interglacials og Interstadialer i Danmarks kvartær. *Medd. fra Dansk Geol. Forening* **15**, 486–506.
- Auken E. and Christiansen A.V. 2004. Layered and laterally constrained 2D inversion of resistivity data. *Geophysics* **69**, 752–761.
- Auken E., Christiansen A.V., Jacobsen B.H., Foged N. and Sørensen K.I. 2005. Piecewise 1D laterally constrained inversion of resistivity data. *Geophysical Prospecting* **53**, 497–506. doi: 10.1111/j.1365-2478.2005.00486.x
- Auken E., Christiansen A.V., Westergaard J.H., Kirkegaard C., Foged N. and Viezzoli A. 2009a. An integrated processing scheme for high-resolution airborne electromagnetic surveys, the SkyTEM system. *Exploration Geophysics* **40**, 184–192. doi: 10.1071/EG08128
- Auken E., Viezzoli A. and Christiansen A.V. 2009b. A single software for processing, inversion, and presentation of AEM data of different systems: the Aarhus Workbench. *ASEG Extended Abstracts*, 1–5.
- Brodie R. and Sambridge M. 2006. A holistic approach to inversion of frequency-domain airborne EM data. *Geophysics* **71**, G301–G312.
- Burschil T., Wiederhold H. and Auken E. 2012. Seismic results as a priori knowledge for airborne TEM data inversion – a case study. *Journal of Applied Geophysics* **80**, 121–128. doi: 10.1016/j.japgeo.2012.02.003
- Christiansen A.V. and Auken E. 2009. Presenting a free, highly flexible inversion code. *EAGE 15th European Meeting of Environmental and Engineering Geophysics*, Dublin.
- Christiansen A.V. and Auken E. 2012. A global measure for depth of investigation. *Geophysics* **77**, WB171–WB177.
- Christiansen A.V., Auken E. and Sørensen K. 2006. The transient electromagnetic method. In: *Groundwater Geophysics – a Tool for Hydrogeology*, (ed. R. Kirsch), 179–225. Springer, Germany.
- d'Ozouville N., Auken E., Sørensen K., Violette S., de Marsily G., Deffontaines B. *et al.* 2008. Extensive perched aquifer and structural implications revealed by 3D resistivity mapping in a Galapagos volcano. *Earth and Planetary Science Letters* **269**, 517–521. doi: 10.1016/j.epsl.2008.03.011
- Dybkjær K. 2011. *Palynologisk undersøgelse af 12 prøver fra boringen DGU nr. 113.1855 ved Vestkærvej, syd for Ølgod*. GEUS notat, 1–11.
- Ellis R.G. and Oldenburg D.W. 1994. Applied Geophysical Inversion. *Geophysical Journal International* **116**, 5–11.
- Friberg R. and Thomsen S. 1999. Kortlægning af Ribe Formationen. *Teknisk Rapport*.
- Gabriel G., Kirsch R., Siemon B. and Wiederhold H. 2003. Geophysical investigation of buried Pleistocene subglacial valleys in Northern Germany. *Journal of Applied Geophysics* **53**, 159–180.
- Houmark-Nielsen M. 2004. The Pleistocene of Denmark: a review of stratigraphy and glaciation history. In: *Quaternary Glaciations – Extent and Chronology*, (eds J. Ehlers and P.L. Gibbard), 35–46. Elsevier.
- Høyer A.-S., Møller I. and Jørgensen F. 2013a. Challenges in geophysical mapping of glaciotectionic structures. *Geophysics* **78**, B287–B303. doi: 10.1190/GEO2012-0473.1
- Høyer A.-S., Jørgensen F., Jacobsen P.R. and Piotrowski J. 2013b. Deeply rooted glaciotectionism in western Denmark: Geological composition, structural characteristics and the origin of Varde hill-island. *Journal of Quaternary Science* **28**, 683–696. doi: 10.1002/jqs.2667
- Høyer A.-S., Lykke-Andersen H., Jørgensen F. and Auken E. 2011. Combined interpretation of SkyTEM and high-resolution seismic data. *Physics and Chemistry of the Earth* **36**, 1386–1397. doi: 10.1016/j.pce.2011.01.001
- Jackson D.D. and Matsu'ura M. 1985. A Bayesian Approach to Nonlinear Inversion. *Journal of Geophysical Research* **90**, 581–591. doi: 10.1029/JB090iB01p00581
- Jørgensen F., Lykke-Andersen H., Sandersen P.B.E., Auken E. and Nørmark E. 2003a. Geophysical investigations of buried Quaternary valleys in Denmark: An integrated application of transient electromagnetic soundings, reflection seismic surveys and exploratory drillings. *Journal of Applied Geophysics* **53**, 215–228. doi: 10.1016/j.japgeo.2003.08.017
- Jørgensen F., Sandersen P.B.E. and Auken E. 2003b. Imaging buried Quaternary valleys using the transient electromagnetic method. *Journal of Applied Geophysics* **53**, 199–213. doi: 10.1016/j.japgeo.2003.08.016
- Kirkegaard C., Sonnenborg T.O., Auken E. and Jørgensen F. 2011. Salinity distribution in heterogeneous coastal aquifers mapped by airborne electromagnetics. *Vadose Zone Journal* **10**, 125–135. doi: 10.2136/vzj2010.0038
- Larsen G. and Kronborg C. 1994. *Geologisk set; Det mellemste Jylland*. Geografforlaget.
- Larsen G. and Sand-Jensen K. 2006. *Naturen i Danmark: Geologien*. Gyldendal, 549.

- Meju M.A. 1994. Biased estimation: a simple framework for inversion and uncertainty analysis with prior information. *Geophysical Journal International* **119**, 521–528.
- Menke W. 1989. *Geophysical Data Analysis: Discrete Inverse Theory*. Academic Press, San Diego,
- Nyboe N.S., Jørgensen F. and Sørensen K. 2010. Integrated inversion of TEM and seismic data facilitated by high penetration depths of a segmented receiver setup. *Near Surface Geophysics* **8**, 467–473.
- Pullan S.E. 2004. The role of geophysics in 3D mapping. *Workshop on Geological Models for Groundwater; Geological Society of America*, Salt Lake City, UT.
- Rasmussen E.S., Dybkjær K. and Piasecki S. 2010. *Lithostratigraphy of the Upper Oligocene – Miocene succession of Denmark*. Geological Survey of Denmark and Greenland Bulletin 22, 92 + 9 plates.
- Rasmussen L.B. 1966. *Biostratigraphical studies on the marine younger Miocene of Denmark; based on the molluscan faunas*. Geological Survey of Denmark and Greenland, 358.
- Sapia V., Oldenborger G. and Viezzoli A. 2012. Incorporating a-priori information into AEM inversion for geological and hydrogeological mapping of the Spiritwood valley aquifer, Manitoba, Canada. *Atti del XXXI Convegno Nazionale del GNGTS*, Potenza, Italy, 194–199.
- Scales J.A. and Tenorio L. 2001. Prior information and uncertainty in inverse problems. *Geophysics* **66**, 389–397. doi: 10.1190/1.1444930
- Sengpiel K.P. and Siemon B. 1997. Groundwater exploration in the Namib Desert using helicopter-borne electromagnetics (Hubschrauberelektromagnetik zur grundwassererkundung in der Namib-Wüste/Namibia). *Zeitschrift für Angewandte Geologie* **43**, 130–136.
- Shivelman V. and Goldman M. 2000. Integration of shallow reflection seismics and time domain electromagnetics for detailed study of the coastal aquifer in the Nitzanim area of Israel. *Journal of Applied Geophysics* **44**, 197–215.
- Steuer A., Siemon B. and Eberle D. 2008. Airborne and ground-based electromagnetic investigations of the freshwater potential in the tsunami-hit area Sigli, Northern Sumatra. *Journal of Environmental and Engineering Geophysics* **13**, 39–48. doi: 10.2113/JEEG13.1.39
- Supper R., Motschka K., Ahi A., Bauer-Gottwein P., Gondwe B., Alonso G.M. *et al.* 2009. Spatial mapping of submerged cave systems by means of airborne electromagnetics: An emerging technology to support protection of endangered karst aquifers. *Near Surface Geophysics* **7**, 613–627. doi: 10.3997/1873-0604.2009008
- Sørensen K.I. and Auken E. 2004. SkyTEM – a new high-resolution helicopter transient electromagnetic system. *Exploration Geophysics* **35**, 191–199.
- Tarantola A. and Valette B. 1982. Generalized nonlinear inverse problems solved using a least squares criterion. *Reviews of Geophysics and Space Physics* **20**, 219–232.
- Teatini P., Tosi L., Viezzoli A., Baradello L., Zecchin M. and Silvestri S. 2011. Understanding the hydrogeology of the Venice Lagoon subsurface with airborne electromagnetics. *Journal of Hydrology* **411**, 342–354. doi: 10.1016/j.jhydrol.2011.10.017
- Tikhonov A.N. and Arsenin V.Y. 1977. *Solutions of Ill-posed Problems*. Winston, 258.
- van der Veen M., Spitzer R., Green A.G. and Wild P. 2001. Design and application of a towed land-streamer system for cost-effective 2-D and pseudo-3-D shallow seismic data acquisition. *Geophysics* **66**, 482–500.
- Vangkilde-Pedersen T., Dahl J.F. and Ringgaard J. 2006. Five years of experience with landstreamer vibroseis and comparison with conventional seismic data acquisition. *Symposium on the Application of Geophysics to Engineering and Environmental Problems (SAGEEP)*, Seattle.
- Vangkilde-Pedersen T., Skjellerup P., Ringgaard J. and Jensen J.F. 2003. Pulled array seismic (PAS) – A new method for shallow reflection seismic data acquisition. *EAGE*, Stavanger.
- Viezzoli A., Auken E. and Munday T. 2009. Spatially constrained inversion for quasi 3D modelling of airborne electromagnetic data an application for environmental assessment in the Lower Murray Region of South Australia. *Exploration Geophysics* **40**, 173–183. doi: 10.1071/EG08027
- Viezzoli A., Christiansen A.V., Auken E. and Sørensen K. 2008. Quasi-3D modeling of airborne TEM data by spatially constrained inversion. *Geophysics* **73**, F105–F113. doi: 10.1190/1.2895521
- Yilmaz Ö. 1987. *Seismic Data Processing*. Society of Exploration Geophysicists, 526.

APPENDIX 1

The inversion problem

The inversion scheme we use here is the scheme of the inversion code AarhusInv (Auken and Christiansen 2004, Christiansen and Auken 2009, Viezzoli *et al.* 2008) used for constrained inversion of geophysical EM and DC data. It is a least squares inversion of a layered earth regularized through spatial constraints, which give smooth lateral transitions. Similarly, a priori information can be added at any point and it will then migrate through the lateral constraints to parameters at adjacent sites. We constrain layer resistivities and depths.

The dependence of apparent resistivity on subsurface parameters is in general described as a non-linear differentiable forward mapping. For data inversion, we follow the established practice of linearized approximation by the first term of the Taylor expansion

$$\mathbf{d}_{obs} - \mathbf{e}_{obs} \cong \mathbf{G} \delta \mathbf{m}_{true} + \mathbf{g}(\mathbf{m}_{ref}) \quad (1)$$

where \mathbf{d}_{obs} is the observed data, \mathbf{e}_{obs} is the error on the observed data and \mathbf{g} is the nonlinear mapping of the model to the data space, and $\delta \mathbf{m}_{true} = \mathbf{m}_{true} - \mathbf{m}_{ref}$. The true model, \mathbf{m}_{true} has to be sufficiently close to some arbitrary reference model, \mathbf{m}_{ref} for the linear approximation to be valid. We choose to apply logarithmic parameters, in order to minimize non linearity and impose positivity.

The Jacobian matrix, \mathbf{G} , contains the partial derivatives of the mapping

$$G_{ab} = \frac{\partial d_a}{\partial m_b} \quad (2)$$

for the a^{th} datum and the b^{th} model parameter.

In short, we write:

$$\mathbf{G} \delta \mathbf{m}_{true} = \delta \mathbf{d}_{obs} - \mathbf{e}_{obs}, \quad (3)$$

where $\delta \mathbf{d}_{obs} = \mathbf{d}_{obs} - \mathbf{g}(\mathbf{m}_{ref})$.

The constraints are connected to the true model as

$$\mathbf{R} \delta \mathbf{m}_{true} = \delta \mathbf{r} + \mathbf{e}_r, \quad (4)$$

where \mathbf{e}_r is the error on the constraints, with 0 as expected value. $\delta \mathbf{r} = -\mathbf{R} \mathbf{m}_{ref}$ claims identity between the parameters tied by constraints in the roughening matrix \mathbf{R} .

By joining equations 3 and 4 we may write the inversion problem as:

$$\begin{bmatrix} \mathbf{G} \\ \mathbf{R} \end{bmatrix} \cdot \delta \mathbf{m}_{true} = \begin{bmatrix} \delta \mathbf{d}_{obs} \\ \delta \mathbf{r} \end{bmatrix} + \begin{bmatrix} \mathbf{e}_{obs} \\ \mathbf{e}_r \end{bmatrix} \quad (5)$$

and adding the option for a priori information we get:

$$\begin{bmatrix} \mathbf{G} \\ \mathbf{R} \\ \mathbf{I} \end{bmatrix} \cdot \delta \mathbf{m}_{true} = \begin{bmatrix} \delta \mathbf{d}_{obs} \\ \delta \mathbf{r} \\ \delta \mathbf{m}_{prior} \end{bmatrix} + \begin{bmatrix} \mathbf{e}_{obs} \\ \mathbf{e}_r \\ \mathbf{e}_{prior} \end{bmatrix} \quad (6)$$

or more compactly

$$\mathbf{G}' \cdot \delta \mathbf{m}_{true} = \delta \mathbf{d}' + \mathbf{e}'. \quad (7)$$

The covariance matrix for the joint observation error, \mathbf{e}' , becomes:

$$\mathbf{C}' = \begin{bmatrix} \mathbf{C}_{obs} & & \underline{\underline{0}} \\ & \mathbf{C}_R & \\ \underline{\underline{0}} & & \mathbf{C}_{prior} \end{bmatrix} \quad (8)$$

where \mathbf{C}_{obs} refers to the observational errors \mathbf{e}_{obs} , \mathbf{C}_R to the error on the constraints \mathbf{e}_r , and \mathbf{C}_{prior} to the error on the a priori information.

The objective function, with ND as the number of data, NC the number of constraints, and NP the number of a priori parameters is:

$$Q = \left(\frac{1}{ND + NC + NP} [(\delta \mathbf{d}'^T \mathbf{C}'^{-1} \delta \mathbf{d}')] \right)^{\frac{1}{2}} \quad (9)$$

the objective function is then minimized by Menke (1989):

$$\delta \mathbf{m}_{est} = (\mathbf{G}'^T \mathbf{C}'^{-1} \mathbf{G}')^{-1} \mathbf{G}'^T \mathbf{C}'^{-1} \delta \mathbf{d}'. \quad (10)$$

This implies that the data misfit, the model roughness (i.e., the constraints), and the a priori information are minimized together.

Estimation of the uncertainty for the model parameters can be obtained by the linearized covariance matrix \mathbf{C}_{est} , calculated from the following expression (Tarantola and Valette 1982):

$$\mathbf{C}_{est} = (\mathbf{G}'^T \mathbf{C}'^{-1} \mathbf{G}' + \mathbf{R}^T \mathbf{C}_R^{-1} \mathbf{R} + \mathbf{C}_{prior}^{-1})^{-1} \quad (11)$$